The Journal of Physical Chemistry A

 VOLUME 101, NUMBER 44, OCTOBER 30, 1997

LETTERS

Photodissociation, Recombination, and Electron Transfer in Cluster Ions: A Nonadiabatic Molecular Dynamics Study of $I_2^-(CO_2)_n$

N. Delaney, J. Faeder, P. E. Maslen,† and R. Parson*

JILA and Department of Chemistry and Biochemistry, University of Colorado and National Institute of Standards and Technology, Boulder, Colorado 80309-0440

Received: July 25, 1997; In Final Form: September 17, 1997[⊗]

We simulate and interpret the photodissociation and recombination of I_2^- embedded in CO_2 clusters using a Hamiltonian that accounts for the strong perturbation of the solute electronic structure by the solvent. The calculated product distributions agree well with the experimental results of Lineberger and co-workers. Excited-state dynamics are more involved than anticipated from the isolated solute potential curves. For example, dissociation does not occur from the A′ state, and permanent recombination occurs only on the X state, despite the fact that the A state of I_2^- is weakly bound. We discuss the role of the cluster environment in bringing about recombination and electronic relaxation in terms of a qualitative model inspired by the theory of electron transfer in solution.

1. Introduction

Although photodissociation and recombination of I_2^- have been extensively studied in clusters[1−6] and solution,[7−11] only recently have simulations appeared that follow the entire course of this simple chemical reaction.[12,13] The challenge of modeling these systems is 2-fold: first, as the anion dissociates, the flow of excess charge couples strongly to the motion of the solvent molecules; second, this charge flow is highly nonclassical, depending sensitively upon the nature of the solute electronic wave function.

Figure 1 illustrates the state dependence of charge flow for a simple two-state model borrowed from the theory of electron transfer in solutions.[14−16] The diabatic potential curves are two intersecting parabolas whose minima represent solvated iodide and neutral iodine. When the solute bond length is near its equilibrium value, the electronic coupling is strong and the adiabatic curves are well-separated energetically, as represented by the dashed curves. As the solvent moves along the lower adiabatic curve, the charge follows the solvent from one side of the solute to the other. However, the charge moves in just the opposite way on the upper adiabatic state. A vertical excitation, as shown in the figure, changes the solute electronic state, moving the charge from I_A to I_B; however, the solvent still surrounds I_A. The solvent moves toward the charge in an effort to reestablish equilibrium. But, as the solvent coordinate crosses zero, and the solvent favors I_B, the electronic state changes character, and the charge returns to I_A. The solvent must change direction once again to pursue the charge. This oscillation, which we have termed "anomalous charge switching",[6,17,12] will persist as long as the solute remains in the excited state. Anomalous charge switching is a direct consequence of the antibonding character of the A′ state; in general we expect antibonding states to polarize in the opposite direction compared to the normal, bonding states.[6] The solid lines in Figure 1 represent a longer solute bond length, where the electronic coupling is weaker and transitions between states can occur when the solvent coordinate is near zero.

In the experiments we model, I_2^- is excited to the anomalous

* Corresponding author. E-mail: rparson@jila.colorado.edu.
† Current address: Department of Chemistry, University of California, Berkeley, CA 94720.
⊗ Abstract published in *Advance ACS Abstracts,* October 15, 1997.

S1089-5639(97)02435-3 CCC: $14.00

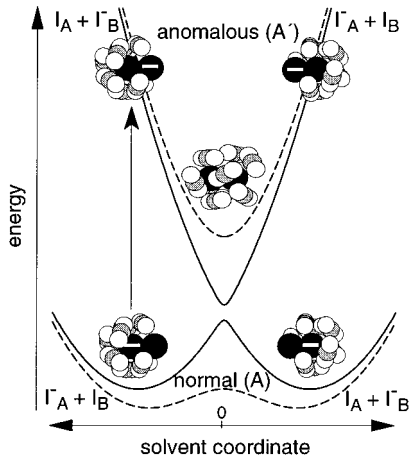

Figure 1. Schematic potential energy surfaces of solvated I_2^-. Dashed lines represent a cross section at small I−I separations, where the bond coupling is strong compared with the solute−solvent interactions. The solid curves represent the weak coupling limit, which arises at longer bond lengths ($R_{solute} > 5$ Å). Anomalous charge switching in the upper curves is illustrated by the cartoons.

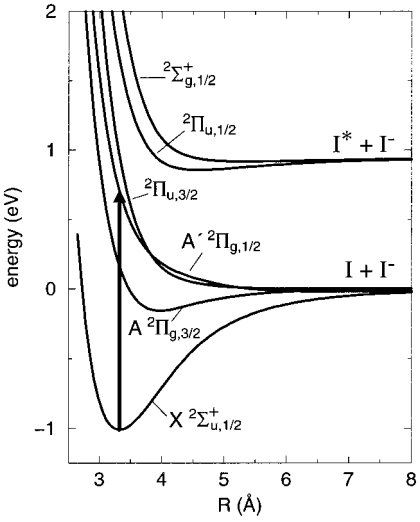

Figure 2. Scaled ab initio gas-phase potential curves for I_2^-. The arrow shows the 790 nm photoexcitation to the A′ $^2\Pi_{g,1/2}$ state modeled in the current simulations.

A′ potential surface by a 790 nm laser pulse, as shown in Figure 2. As the solute dissociates, it can undergo nonadiabatic electronic transitions to normal charge switching A and X states, where the dynamics of the charge−solvent interaction will change dramatically. We have recently developed a model Hamiltonian to compute the multiple, highly coupled potential energy surfaces that arise in these ionic systems.[12] In this Letter we present nonadiabatic molecular dynamics simulations of photodissociation and recombination in I_2^- clustered with 4−16 CO_2 molecules, an extension of our recent work on $I_2^-Ar_n$ clusters.[12] We observe for the first time the complete excited-state dynamics and identify the pathways for electronic relaxation and subsequent product formation. The CO_2 clusters behave quite differently from the previously studied argon clusters[12] because of the much stronger solute−solvent interactions.

2. Methods

We determine the interaction potential between the solute I_2^- and the solvent CO_2 molecules using a model Hamiltonian described previously.[12] This model includes state-dependent electrostatic and induction interactions between the solute and solvent based on ab initio calculations of the solute wave functions[18] and experimental data for the solvent charge distribution[19] and polarizability.[20] State independent atom−atom Lennard-Jones potentials account for the remaining dispersion and repulsion interactions and are fit to reproduce the known I^-−CO_2 and I−CO_2 potential curves.[21] The CO_2−CO_2 interaction potential is taken from Murthy *et al.*[19] The model captures the sensitive dependence of the solute charge distribution on the solute electronic state, the solute bond length, and the positions and orientations of the solvent molecules. A more comprehensive discussion of the model along with comparison to other semiempirical methods is currently in preparation.[22]

The methods for determining cluster structures, preparing initial ensembles, and computing the nonadiabatic dynamics following photodissociation have also been described previously.[12] Nuclear motion on a single potential surface is computed using the velocity version of the Verlet algorithm,[23] while hopping between electronic states of the solute is computed using Tully's method[24,25] with some minor modifications.[12]

For each cluster size studied, 41 trajectories were computed from starting configurations obtained by sampling a single 400 ps trajectory with an average temperature of 80 K. This temperature was chosen to lie on the upper end of the solid−liquid phase transition region in the clusters, on the basis of our previous experience that such temperatures gave reasonable agreement with experimental results.[12] The products are determined by integrating the trajectories until the nuclear configurations meet either of two criteria: the I−I distance exceeds 20 Å, or I_2^- undergoes more than 100 oscillations in a particular potential well. The dissociation and recombination times vary from a few picoseconds to over 100 ps in some cases where I_2^- is trapped in an excited electronic state before recombining. The time scale for evaporation of CO_2 molecules from the clusters following photodissociation appears to be much longer than the 50−100 ps over which the trajectories are integrated, and thus we do not calculate the final product mass distributions, which are measured experimentally at 5−10 μs.[2,4]

3. Results and Discussion

Figure 3a shows three cluster structures obtained from 80 K ensembles. The average binding energy per CO_2 at 80 K is fairly constant at about 200 meV for $10 \leq n \leq 18$, while for smaller cluster sizes it dips to about 190 meV. These values are consistent with the upper bound of 250 meV estimated from experiment that includes the kinetic energy released upon evaporation.[2] The clusters develop a pronounced asymmetry in the range $7 \leq n \leq 13$, which is illustrated by the middle structure at $n = 10$. More symmetric solvent configurations are shown at $n = 5$, where the solvent tends to clump about the waist of I_2^-, and $n = 16$, the size at which the first solvation shell is thought to close in the experiment.[2] The structures and energetics we observe in our 80 K ensembles are in good agreement with earlier studies using optimized geometries.[6,26,27]

To quantify the degree of solvent asymmetry, we define a solvent coordinate, $\Delta\Phi$, as the change in energy when a charge of $-e$ is moved from I_A to I_B for a fixed nuclear configuration. The average magnitude of $\Delta\Phi$ in the 80 K ensembles peaks at $n = 10$ and is a factor of 5 smaller for $n = 16$, as shown in Figure 3a. Large values of $\Delta\Phi$ exert a strong force to localize the charge on the favored atom, so that in the most asymmetric configurations, 60% of the excess charge in ground-state I_2^- resides on the favored end of the molecule. Large initial solvent asymmetries also strongly influence the dynamics following photodissociation, as we discuss below.

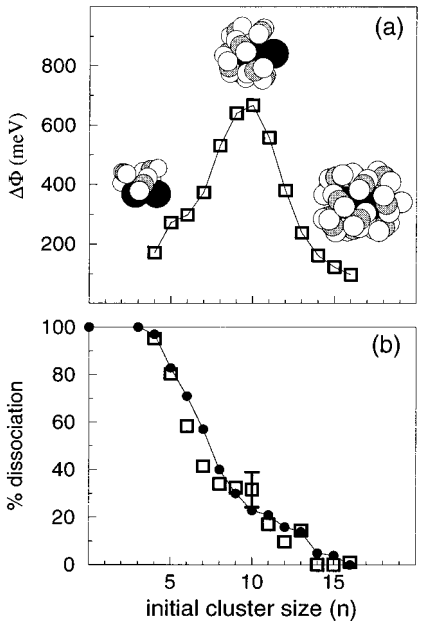

Figure 3. (a) Ensemble average of the magnitude of the solvent coordinate as a function of cluster size. Typical structures for $n = 5$, 10, 16 are shown. (b) Branching ratio for the products of $I_2^-(CO_2)_n$ photodissociation at 790 nm. The filled circles are the experimental data, and the squares show the simulation results. The 1σ error bar shown for $n = 10$ is based on the statistical sampling and is representative of the error bars at other cluster sizes.

Figure 3b compares the product branching ratios calculated from the model with the experimental results of Vorsa et al.[4,28] The 1σ error bar shown results from sampling a relatively small number of trajectories—41 for each cluster size. The discrepancies between simulation and experiment are within the uncertainties for all but a few cluster sizes, and thus the model accurately reproduces the rapid onset of caging with increasing cluster size observed in the experiments.[2,4] Also in agreement with experiment are the results that all of the dissociated products arise from ejection of neutral I atoms leaving behind solvated I^-, while all of the recombined products are based on I_2^- in its ground electronic state. In contrast, for argon clusters experiment[4] and simulation[12,13] find additional product channels corresponding to ejection of I^- ions and to recombination of I_2^- in the A state.

In Figure 4 we plot the trajectories for $n = 9$ and 16 in two dimensions: the solute bond length and $\Delta\Phi$. The three panels shown for each cluster size partition the trajectories based on electronic state. All trajectories begin in the A′ state, shown in the top panel, at $R_{solute} = 3.3$ Å. Upon reaching the coupling regions marked with ovals, trajectories make transitions to the lower-lying A and X states, shown on the left and right, respectively. Transitions between these two lower states can also occur in the regions outlined with rectangles. For simplicity, we do not show the dynamics on the $^2\Pi_{u,3/2}$ state; it is accessible from the A′ state and exhibits anomalous charge switching.

A main feature of the dynamics on the A′ state is the narrow range of solvent coordinates observed in the coupling regions. One might expect that as R_{solute} increases the charge and solvent would tend to localize on a single iodine atom. But the A′ surface has anomalous character, so that, as depicted in Figure 1, solvent asymmetry creates charge flow toward the less solvated atom, which in turn pulls the solvent back toward more symmetric configurations. Anomalous charge switching thus creates a steep valley on the A′ potential surface, funneling trajectories into symmetric solvent configurations. The $n = 16$ trajectories begin with a fairly narrow range of solvent asymmetries that tightens somewhat upon dissociation. The funnel shape is more striking for $n = 9$, where there is a much broader range of initial solvent coordinates. For large initial $\Delta\Phi$, the charge jumps to the escaping atom, which slows down and pulls solvent molecules away from the other atom until the solvent configuration becomes nearly symmetric.

Anomalous charge switching also prevents dissociation on the A′ state, because the attraction of the CO_2 to I^- is so strong that the negative ion cannot escape. The A′ funnel thus has a well in the dissociation coordinate that traps the trajectories in a region where the R_{solute} is about 5−7 Å. The maximal extension of the solute bond in the A′ state is somewhat larger on average for $n = 9$ than $n = 16$, but dissociation cannot occur in either case or for any of the cluster sizes studied. In contrast, much larger separations and even I^- ejection were observed in simulations of comparable cluster sizes in $I_2^-Ar_n$.[12,13]

Following the concerted dynamics in the A′ state, electronic relaxation to the X and A states generally takes place less than 1 ps after photoexcitation. The effect of returning to a normal charge switching state is dramatic: charge localizes completely onto one solute atom and the solvent races to the ion, increasing the magnitude of $\Delta\Phi$ to 1 eV or more within 200−500 fs. Meanwhile, R_{solute} hardly changes. The disparity in response time of the solvent and the solute often results in a solvent-separated pair with CO_2 molecules tightly clustered to I^- and the I atom residing on the surface. These pairs, which were not observed in simulations of $I_2^-Ar_n$ clusters,[12,13] eventually either dissociate, via thermal evaporation of I, or recombine on the X state.

Trajectories are often trapped for extended periods in the A state prior to recombination or dissociation, as shown in Figure 4. A state trapping is observed rarely in small clusters but is common in cluster sizes $n \geq 7$. Both the frequency and length of trapping increase with cluster size. Residence times of 5−25 ps are typical, but product formation can require as long as 50−100 ps. In addition to solvent-separated pairs, we observe transient recombination of I_2^-; that is, some trajectories pass within $R_{solute} = 4$ Å, the equilibrium bond length, on the A state. However, the excited-state I_2^- bond is weak compared to the $I^-\cdots CO_2$ interaction, and the bond is broken before appreciable vibrational relaxation can occur. Nevertheless, these metastable cluster configurations contribute to the long lifetimes on the A state.

Formation of recombined products following trapping on the A state requires a coordinated sequence of events. The A state and the X state differ by the alignment of the empty p orbital on iodine. For $R_{solute} > 5$ Å, the alignment of that orbital is readily altered by collisions with solvent molecules,[12,29] causing electronic transitions back and forth between these two states. To get recombination on the ground state, the solute bond length must increase for the orbital to be realigned; simultaneously, neutral iodine must break into the first solvation shell, displacing CO_2.

On the ground state, the covalent bond is roughly an order of magnitude stronger than on the A state and is comparable in size to the total solute−solvent interaction. Once a trajectory reaches 5−6 Å on the X state, the strong bond force draws I_2^- back together; the solute rapidly recombines, and the magnitude of the solvent coordinate never exceeds 0.5 eV thereafter. Trajectories that hop from the A′ state to the X state at short bond lengths recombine directly in roughly 1−3 ps, without forming the solvent-separated pair.

There are two pathways for I_2^- dissociation. During trapping on the A state, neutral iodine is the most weakly bound species

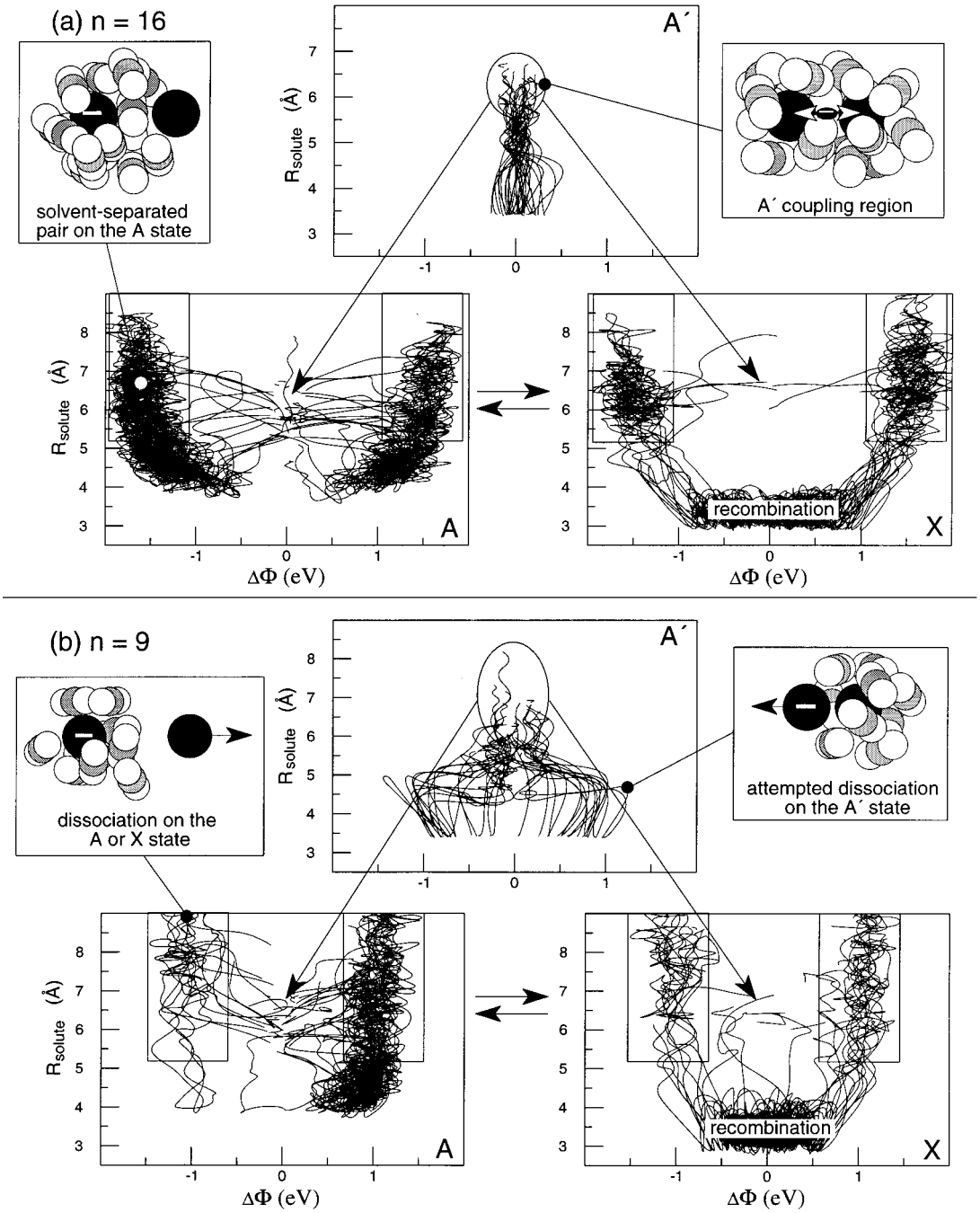

Figure 4. Dynamics of an ensemble of 41 trajectories projected onto the solute bond length and the solvent coordinate for $n = 16$ (a) and $n = 9$ (b). Trajectories begin in the A′ state at $R_{solute} = 3.3$ Å and undergo transitions to the lower states in the regions indicated with ovals. A↔X coupling regions are marked with rectangles. The apparent favoring of the right side of the A state in (b) is due to the few trajectories that remain trapped for a long time.

in the cluster and therefore readily evaporates. This is the dominant dissociation mechanism for $n \geq 9$. In the smaller clusters, dissociation is generally more direct, with R_{solute} increasing monotonically following the transition from the A′ state. Direct dissociation arises because there are fewer solvent molecules to hold the solute atoms together.

4. Conclusions

In summary, photoexcitation of I_2^- with a 790 nm photon places the solute on the A′ electronic surface, which like the anomalous curves in Figure 1 funnels the trajectories into highly symmetric solvent configurations as I_2^- dissociates. Following electronic relaxation, the A and X surfaces, like the normal charge switching curves in Figure 1, pull the trajectories toward highly asymmetric solvent configurations. The electronic coupling on the A state is small, and the strong solute−solvent interactions destabilize the weak I_2^- bond, allowing formation of long-lived solvent-separated pairs. Eventually, trajectories in the A state either dissociate or hop to the X state, where the much larger electronic coupling creates a strong pull toward permanent recombination, which occurs rapidly if $R_{solute} \leq 5-6$ Å. The strong ground-state I_2^- bond also leads to direct recombination within a few picoseconds for a significant fraction of trajectories.

The results presented here emphasize that the isolated I_2^- potential curves can be misleading when interpreting the dynamics of photodissociation and recombination in CO_2 clusters. When CO_2 is present, for example, the A′ state is not

dissociative and also I_2^- cannot recombine permanently in the A state. Previous analysis of pump−probe experiments in these clusters[3,5] has used the isolated curves to locate the Franck−Condon regions for probe absorption. Our results suggest that coupling to the solvent will shift these regions significantly, possibly leading to new interpretations of the experimental signals and the dynamics. Finally, while it is the large solvent asymmetry of the cluster environment that produces the interesting dynamics we report here, we anticipate that these effects may be an amplification of phenomena that occur in the liquid phase as a result of solvent fluctuations.

Acknowledgment. We thank Sreela Nandi and John Papanikolas for their contributions to this project. This work was supported by the National Science Foundation under Grants CHE-9217693 and PHY-9512150, and by the National Center for Supercomputing Applications (NCSA) under Grant CHE970015N for computing time on the Silicon Graphics Power ChallengeArray at the NCSA, University of Illinois at Urbana-Champaign.

References and Notes

(1) Perera, L.; Amar, F. G. *J. Chem. Phys.* **1989**, *90*, 7354. These authors simulated photodissociation of Br_2^- using a classical model for charge localization and emphasized the importance of charge switching.

(2) Papanikolas, J. M.; Gord, J. R.; Levinger, N. E.; Ray, D.; Vorsa, V.; Lineberger, W. C. *J. Phys. Chem.* **1991**, *95*, 8028.

(3) Papanikolas, J. M.; Vorsa, V.; Nadal, M. E.; Campagnola, P. J.; Buchenau, H. K.; Lineberger, W. C. *J. Chem. Phys.* **1993**, *99*, 8733.

(4) Vorsa, V.; Campagnola, P. J.; Nandi, S.; Larsson, M.; Lineberger, W. C. *J. Chem. Phys.* **1996**, *105*, 2298.

(5) Vorsa, V.; Nandi, S.; Campagnola, P. J.; Larsson, M.; Lineberger, W. C. *J. Chem. Phys.* **1997**, *106*, 1402.

(6) Papanikolas, J. M.; Maslen, P. E.; Parson, R. *J. Chem. Phys.* **1995**, *102*, 2452.

(7) Banin, U.; Waldman, A.; Ruhman, S. *J. Chem. Phys.* **1992**, *96*, 2416.

(8) Benjamin, I.; Banin, U.; Ruhman, S. *J. Chem. Phys.* **1993**, *98*, 8337.

(9) Kliner, D. A. V.; Alfano, J. C.; Barbara, P. F. *J. Chem. Phys.* **1993**, *98*, 5375.

(10) Walhout, P. K.; Alfano, J. C.; Thakur, K. A. M.; Barbara, P. F. *J. Phys. Chem.* **1995**, *99*, 7568.

(11) Benjamin, I.; Barbara, P. F.; Gertner, B. J.; Hynes, J. T. *J. Phys. Chem.* **1995**, *99*, 7557.

(12) Faeder, J.; Delaney, N.; Maslen, P.; Parson, R. *Chem. Phys. Lett.* **1997**, *270*, 196.

(13) Batista, V. S.; Coker, D. F. *J. Chem. Phys.* **1997**, *106*, 7102.

(14) Marcus, R. A. *Annu. Rev. Phys. Chem.* **1964**, *15*, 155.

(15) Newton, M. D.; Sutin, N. *Annu. Rev. Phys. Chem.* **1984**, *35*, 437.

(16) Schatz, G. C.; Ratner, M. A. *Quantum Mechanics in Chemistry*; Prentice Hall: Englewood Cliffs, NJ, 1993; Chapter 10.

(17) Maslen, P. E.; Papanikolas, J. M.; Faeder, J.; Parson, R.; ONeil, S. V. *J. Chem. Phys.* **1994**, *101*, 5731.

(18) Maslen, P. E.; Faeder, J.; Parson, R. *Chem. Phys. Lett.* **1996**, *263*, 63.

(19) Murthy, C. S.; O'Shea, S. F.; McDonald, I. *Mol. Phys.* **1983**, *50*, 531.

(20) Gray, C. G.; Gubbins, K. E. *Theory of Molecular Fluids*; Clarendon: Oxford, 1984; Vol. 1.

(21) Zhao, Y.; Arnold, C. C.; Neumark, D. M. *J. Chem. Soc., Faraday Trans.* **1993**, *89*, 1449.

(22) Faeder, J.; Maslen, P. E.; Parson, R. To be submitted.

(23) Andersen, H. C. *J. Comput. Phys.* **1982**, *52*, 24.

(24) Tully, J. C. *J. Chem. Phys.* **1990**, *93*, 1061.

(25) Hammes-Schiffer, S.; Tully, J. C. *J. Chem. Phys.* **1994**, *101*, 4657.

(26) Papanikolas, J. M. I_2^- photodissociation and cage recombination dynamics in size-selected $I_2^-(CO_2)_n$ clusters. Ph.D. Thesis, University of Colorado, 1994.

(27) Amar, F. G.; Perera, L. *Z. Phys. D* **1991**, *20*, 173.

(28) Vorsa, V. Photodissociation dynamics of mass-selected anions and anionic clusters. Ph.D. Thesis, University of Colorado, 1996.

(29) Krylov, A. I.; Gerber, R. B.; Coalson, R. D. *J. Chem. Phys.* **1996**, *105*, 4626.